Development of High-Density Radio Frequency Plasma Sources With Very Small Diameter for Propulsion

Shunjiro Shinohara, Daisuke Kuwahara, Takamichi Ishii, Hiraku Iwaya, Shuichi Nishimura, Tomoya Yamase, Daisuke Arai, and Hirotaka Horita

***Abstract*— Radio frequency (RF) plasma sources, especially helicon ones, are very useful in many fields, because of the high-density (up to $\sim 10^{13}$ cm^{-3}) and low electron temperature (from a few to several electronvolts) available, using an RF frequency range. Here, we develop and characterize very small-area (from 2-cm down to 0.1–0.3 cm in diameter) RF sources that are useful for a space propulsion system with an advanced concept of an electrodeless condition (no direct contact between the plasma and electrodes), leading to a longer operation lifetime. Measurements by using electrostatic probes as well as by a spectrometer based on the collisional radiative model in a small plasma region were employed to estimate the electron density n_e and its temperature. Here, n_e was measured as a function of the input RF power and RF excitation frequency, especially in a higher frequency range than the usual one of ∼14 MHz, under the mirror magnetic-field configuration. The electron cyclotron resonance effect in the divergent field was examined under a weaker magnetic field with the RF frequency lower than those generally employed. The particle production efficiency, even in this small source, showed an excellent performance, based on classical diffusion discussions. In addition, applying these sources were applied to a space propulsion system with the concept of the m (azimuthal mode number) = 0 half-cycle acceleration, which was operated under all electrodeless conditions in both the plasma generation and electromagnetic acceleration phases.**

***Index Terms*— Helicon, plasma production, plasma propulsion, radio frequency (RF).**

Manuscript received September 8, 2017; revised November 5, 2017; accepted November 16, 2017. Date of publication December 7, 2017; date of current version February 9, 2018. This work was supported in part by the Grant-in-Aid for Scientific Research from the Japan Society for the Promotion of Science, under Grant S: 21226019 and Grant B: 17H02295 and in part by NIFS budget code under Grant NIFS17KLER063. The review of this paper was arranged by Senior Editor S. J. Gitomer. *(Corresponding author: Shunjiro Shinohara.)*

S. Shinohara and D. Kuwahara are with the Division of Advanced Mechanical Systems Engineering, Institute of Engineering, Tokyo University of Agriculture and Technology, Tokyo 184-8588, Japan (e-mail: sshinoha@cc.tuat.ac.jp; dkuwahar@cc.tuat.ac.jp).

T. Ishii is with IHI Corporation, Tokyo 135-8710, Japan (e-mail: ishii.iiishi.7@gmail.com).

H. Iwaya is with Sony Corporation, Tokyo 108-0075, Japan (e-mail: iwatanikai@gmail.com).

S. Nishimura, T. Yamase, and D. Arai are with the Department of Mechanical Systems Engineering, Graduate School of Engineering, Tokyo University of Agriculture and Technology, Tokyo 184-8588, Japan (e-mail: s169544t@st.go.tuat.ac.jp; s163270z@st.go.tuat.ac.jp; s176701w@st.go.tuat.ac.jp).

H. Horita is with the Department of Industrial Technology and Innovation, Graduate School of Engineering, Tokyo University of Agriculture and Technology, Tokyo 184-8588, Japan (e-mail: s172285x@st.go.tuat.ac.jp).

Color versions of one or more of the figures in this paper are available online at http://ieeexplore.ieee.org.

Digital Object Identifier 10.1109/TPS.2017.2776110

I. Introduction

HIGH-DENSITY (electron density n_e up to 10^{13} cm^{-3}), low electron temperature T_e ranging from a few to several electronvolts, radio frequency (RF) plasma in a low-pressure region, such as helicon plasma (HP) [1], [2] or inductively coupled plasma (ICP) [3], has been proven to be very effective for use in fundamental research as well as various additional applications. This is because HP can be produced with a broad range of external operating parameters—such as the fill gas pressure P_0, the magnetic-field strength B, and its field configuration—as long as the excitation frequency f is between the ion and electron cyclotron frequencies, i.e., f_{ci} and f_{ce}, respectively. ICP or magnetized ICP (MICP), where in the latter no helicon wave is excited even with the application of a magnetic field, can also have high-density plasmas, which are mostly independent of the external conditions with a simple experimental setup. Therefore, for potential future applications, it is important to extend the dimensions and broaden the external, operational parameters of HP or ICP (and MICP) sources and perform their detailed characterization.

Concerning high-density HP (and MICP) production, we have developed helicon sources of various sizes [4], [5] with a very wide range of plasma diameters D between 2 and 74 cm, using a large HP device [6], [7] and a small helicon device (SHD) [8], which can change plasma diameter flexibly. Recently, we have further reduced D down to 0.3 cm [9], [10], by changing f in a wide range, although plasma characterization was insufficient. Historically, the smallest D achieved by us was 2.5 cm [11], followed by 2 cm [12] at a low pressure (P_0 significantly less than a few pascal). Note that $D = 0.42$ cm was realized [13] with $n_e > 10^{12}$ cm^{-3} but under a high P_0 condition of the order of ∼100 Pa without the magnetic field, in the so-called capacitively coupled plasma (CCP) mode [3].

For deep space propulsion, electric propulsion systems have an advantage over chemical systems in their specific impulse (the ratio of the exhaust velocity to the gravitational acceleration), showing their much better fuel efficiency. However, many of the conventional electric thrusters [14]–[17], where electrodes are exposed to plasmas, suffer from the problems of a finite lifetime caused by the erosion of the electrodes and of worse plasma performance due to contamination of the plasmas with impurities. Therefore, electrodeless operation (no direct contact between the electrodes and the plasma) is

crucial. HP and ICP (and MICP) can be ideal sources for this electrodeless operation, as antenna electrodes are outside the plasmas, separated by insulation materials. In addition, the acceleration method for the target plasma produced must have an electrodeless condition for a long operation lifetime.

However, there have been few trials for the use of electrodeless conditions in the generation and acceleration phases, e.g., the VAriable Specific Impulse Magnetoplasma Rocket project [18], [19] and Helicon Electrodeless Advance Thruster (HEAT) project [4], [5], [20]. The former project utilizes ion cyclotron resonance (ICR) heating [21] for plasma acceleration with a slow-wave heating scheme (so-called a magnetic beach concept), utilizing HP as a target. In this scheme, because of the conservation of the magnetic moment, the perpendicular ion energy increased by the ICR heating is converted to parallel ion energy in the divergent magnetic-field configuration. We proposed other several acceleration schemes [4], [5], such as the rotating magnetic field (RMF) and m (azimuthal mode number) $= 0$ half-cycle acceleration methods.

In this paper, bearing in consideration of future plasma thrusters with electrodeless conditions, we describe the recent development and characterization of very small-diameter RF plasmas such as HP and MICP, as well as a trial of $m = 0$ acceleration of small HP as one of the electromagnetic acceleration methods. Small sources with a high-density and high plasma flow are very useful for long-term operation near Earth such as attitude control; for the use as a neutralizer (electron emission); for obtaining a basic understanding of a future deep-space propulsion, in addition to industrial engineering fields such as the inner coating of small tubes and material development using localized plasma-wall interaction.

Considering other plasma propulsion systems on a small scale, our HP and MICP systems offer the following advantages.

1) As previously mentioned, the electrodeless operation in our systems is very attractive for a long lifetime, which cannot be obtained using other plasma sources.
2) n_e for the present systems is significantly higher (typically more than two orders of magnitude) than that for other sources, which is beneficial for the plasma production efficiency. The first two terms shown earlier can also be applied to large-scale systems.
3) Even at 0.1-cm scale, RF discharges in our system are demonstrated to be possible, as shown later. On the other hand, on this small scale, it is difficult to have direct-current and microwave discharges.
4) While f can be flexibly chosen in our system, as previously mentioned, for an ion propulsion system using electron cyclotron resonance (ECR) discharges [3], [21], $f = f_{ce}$ must be satisfied in the plasma region, which shows a strong restriction between B and f.

Although we have mentioned advantages of our proposed system, needless to say, technically a trial of investigating weight and size (and RF noise) reductions of RF power supply and an impedance-matching circuit, along with improving efficiencies—such as the thrust efficiency—must be considered.

This paper is organized as follows. In Section II, the experimental setup and plasma diagnostics, which are indispensable for plasma characterization, are presented. Here, the experiments focus on two cases: 1) the characterization of plasma with a small diameter of $D = 2$ cm, considering the optimum f condition and magnetic-field configurations, as the direct probe measurement of n_e is possible, and 2) trials to obtain discharges with a very small diameter ($D = 0.1$ and 0.3 cm), along with new optical diagnostics. Regarding the aforementioned objectives, in Section III-A, the detailed characterization of plasmas with a small D of 2 cm is presented, by considering the wide RF frequency range of 7 to 145 MHz for production optimization (mirror magnetic-field configuration). In addition, in Section III-B, using the $D = 2$ cm discharge tube, plasma production with the ECR scheme (divergent magnetic field configuration, using the so-called magnetic beach concept), where $f = f_{ce}$ is satisfied in a plasma region, was attempted. Usually, in low-temperature plasma, $f = 2.45$ GHz, which lies in an ultra high frequency (UHF) region, corresponding to $B = 0.0875$ T, is used for this resonance of $f = f_{ce}$ (in some cases, UHF region of $f = 915$ MHz was used, see, e.g., [22]). However, we examined this plasma production behavior with a weaker field of $B = 0.0155$ T and $f = 435$ MHz [very high frequency (VHF) region], for the use of a simple antenna, which is useful for small sources, instead of a large and heavy waveguide. The weak-magnetic field operation allows the flexible choice of permanent magnets (and electromagnets) and allows lighter magnets to be used.

Trials for plasma production of $D = 0.1$ cm (the smallest plasma diameter, to our knowledge) and 0.3 cm are presented in Section IV, again considering a wide range of f: 12 up to 435 MHz. With this very small diameter, it is difficult to measure the plasma parameters using electrostatic probes, because the size of the probe head is comparable to the plasma diameter D. To overcome this, we developed a collisional radiative (CR) model [23], [24] to estimate n_e and T_e using various Ar I line intensities. In Section V, we presented the $m = 0$ half-cycle acceleration experiment performed with a low ($\sim$10 A range) and high ($\sim$100 A range) antenna current in an electrodeless condition. Increases of the ion velocity v_i as well n_e were observed. Finally, in Section VI, concluding remarks are presented.

II. Experimental Setup

In this section, the experimental setup, i.e., the vacuum and RF systems and magnetic-field configuration for small-diameter RF plasma production are presented, along with the plasma diagnostics. Fig. 1 shows SHD [8] in carrying out the present experiments.

The vacuum system of the SHD consists of four parts: a gas-feeding part, a discharge tube, a vacuum chamber, and a gas pumping part. Argon gas is supplied using a mass flow controller. The discharge tube, which is made of a quartz and has an axial length of 45.3 cm mostly, is connected to a vacuum chamber. Here, the inner diameter (i.d.) of the tubes can be easily changed between 0.1 and 2 cm. In addition, the head flange has ionization or Pirani vacuum gauges to

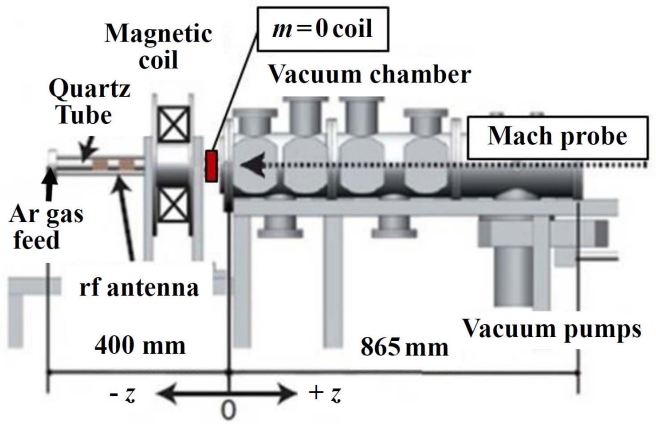

Fig. 1. Schematic of the SHD [8].

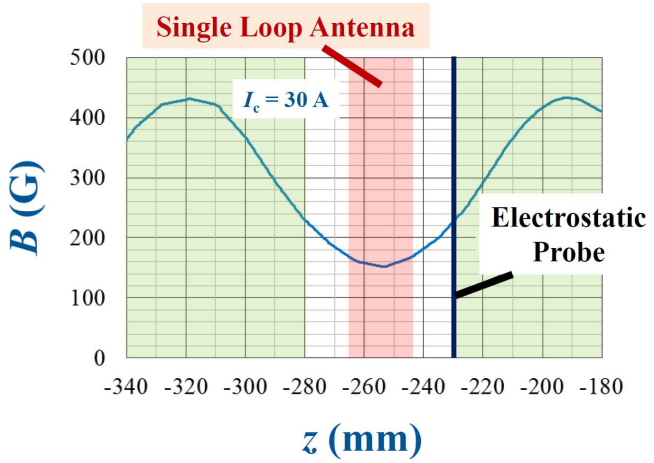

Fig. 2. Mirror magnetic-field configuration with two magnetic-field coils (greenish-yellow regions), a single loop antenna (pink region), and an electrostatic probe.

measure the neutral gas pressure. The vacuum chamber, which has an i.d. of 16.5 cm and an axial length of 86.5 cm, serves as a buffer tank for the discharge tube. A turbo-molecular pump and a rotary pump are connected to the end section of the vacuum chamber, and an ionization gauge is installed near the turbo-molecular pump. The base pressure in the vacuum chamber is $< 10^{-4}$ Pa.

The RF system consists of three parts: a loop or helical antennas for plasma production, an impedance-matching circuit (lumped or distributed constant systems), and an RF power supply. Depending on the experimental conditions, we selected the following power supplies: a variable f between 0.3 and 13.56 MHz with RF power of $P_{RF} = 2$ kW, a variable f between 50 and 150 MHz with $P_{RF} = 1$ kW, and $f = 145$ (435) MHz with $P_{RF} = 350$ (250) W. Unless otherwise stated, except for the case of excitation at $f = 435$ MHz, where continuous operation was employed, a 0.1 s RF pulse was applied to an antenna with a 1 s interval (the duty ratio was 10%).

To excite the helicon wave, a steady external magnetic field is necessary. We have two types of two magnetic-field coils: larger [8] (smaller) one with 9 cm (4.9 cm) i.d. bore can supply up to 825 (440) G for the coil current of $I_c = 30$ A.

To characterize the plasma performance, the n_e profiles were measured using Langmuir or a Mach probes. The latter can also measure the ion flow velocity v_i, under the assumption of a nonmagnetized model [25], [26]. Here, in the case of no T_e measurement, n_e was derived from the ion saturation current under the assumption of the typical T_e of 5 eV. When the discharge tube is small, e.g., <1-cm i.d., electrostatic probes significantly disturb the plasma production, because the probe head occupies a large area in the inner space of the discharge tube. Therefore, noninvasive spectroscopic measurements were performed using a charge coupled device spectrometer (HR2000+, Ocean Optics: 360–752 nm range with a wavelength resolution of 0.5 nm): n_e and T_e were estimated according to the CR model, as previously mentioned.

III. Plasma Characteristics With $D = 2$ cm

In this section, we present the mirror and the divergent magnetic-field configurations, for a $D = 2$ cm quartz tube with an axial length of 45.3 cm. The former utilized a wide range of f (7–435 MHz), which was achieved by changing the gas flow rate, and the latter was focused on the ECR condition with a weaker magnetic field of less than a few 100 G and a lower frequency of 435 MHz than is generally used, as previously mentioned. In [9], concerning the former case, we obtained the data in the convergent field configuration (a double-loop antenna and a measuring point upstream from the magnetic-field coil), and f was only varied among 7, 50, and 70 MHz. Moreover, there was only one case of upstream pressure of ~2 Pa with a gas flow rate of 20 sccm.

A. Mirror Field Configuration

To observe a different behavior from the previous one [9] and determine whether better data can be obtained or not, the mirror magnetic field configuration, which is expected to have better confinement in the mirror region, was used, as shown in Fig. 2. Two small magnetic-field coils with the same current of $I_c = 30$ A were used. A single loop antenna with an axial length of 2 cm (and an electrostatic probe) was located on slightly downstream from the trough of the field. Here, $z = 0$ represents the left-hand side (LHS) of the end of the vacuum chamber, as shown in Fig. 1.

Fig. 3 shows four cases of gas flow rate (1, 5, 10, and 20 sccm) with six f values: 7, 12, 50, 70, 140, and 435 MHz. Here, we observe the following results.

1) In most cases, with P_{RF} exceeding several hundreds of Watt, a high n_e of $> 10^{12}$ cm^{-3} can be obtained in spite of the small radius ($D = 2$ cm).
2) With the increase in f, a threshold power P_{th} for, so-called, a density jump (a steep density rise due to an increase in P_{RF}) decreased.
3) Before the density jump, n_e for a higher f range was higher. In this low power range below a few hundreds of Watt, an f of 70 MHz [Fig. 3(a)] or 140 MHz [Fig. 3(b)–(d)] was better.
4) At the lower gas flow rate, only a higher f of >50 MHz could initiate the plasma, as shown in Fig. 3(a) and (b). In some cases, plasma can be generated with $P_{RF} < 10$ W in the higher f range.

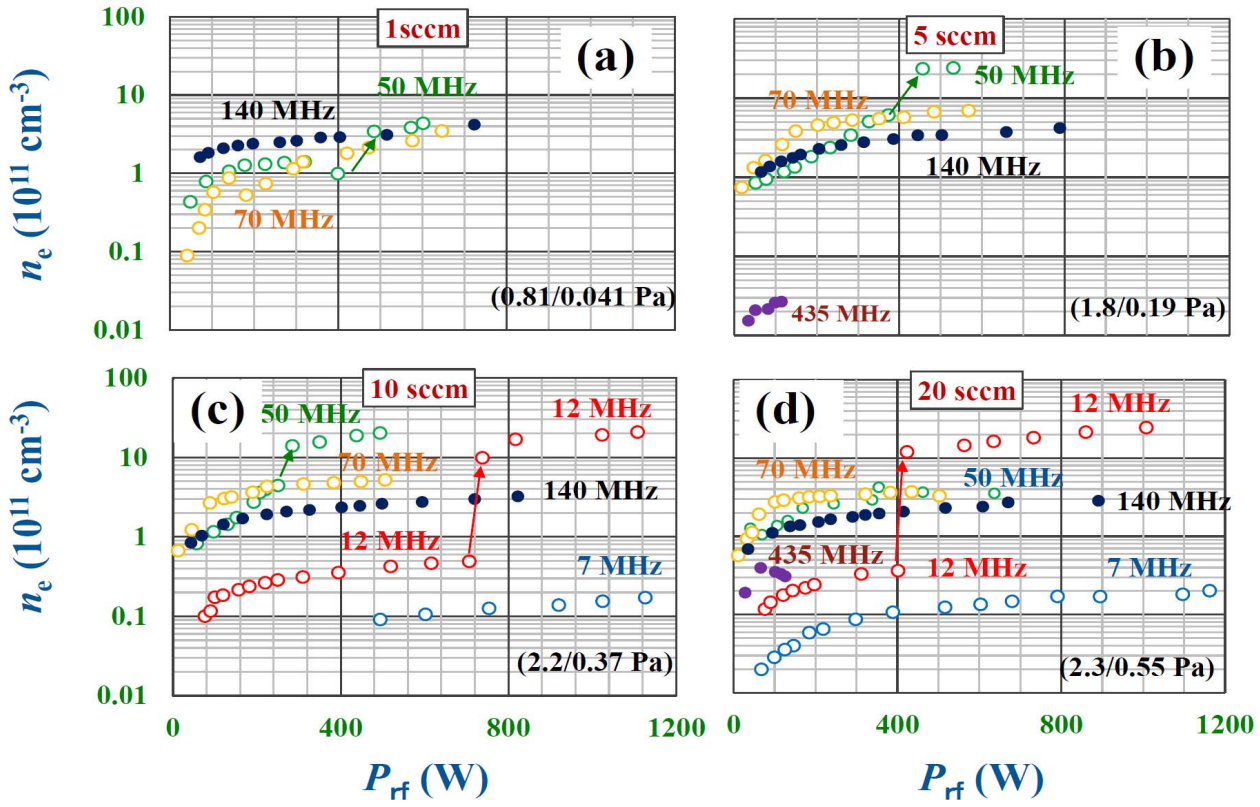

Fig. 3. Electron density n_e as a function of the RF input power P_{RF}, changing argon gas flow rate [(a) 1, (b) 5, (c) 10, and (d) 20 sccm] and RF generation frequency f. Here, the fill pressures in the upstream and the downstream regions of the discharge tube are shown in parentheses.

Nakagawa *et al.* [9] showed a similar trend to 1), but 2) and 3) were not clearly observed. In addition, n_e was slightly smaller but is not significantly different from that in the present one, although the strength of B and the positions of the antenna and Langmuir probe differed.

Here, without the magnetic field case, the same tendencies as the case of the presence of the magnetic field with $I_c = 30$ A case were obtained. However, no generation of the plasma was found in the case of $f = 7$ and 12 MHz, and obtained n_e was slightly smaller (not shown).

B. Divergent Field Configuration, Focusing on ECR Effect

To investigate the ECR phenomena, in the divergent field configuration, n_e was measured, while the magnetic-field coil current and a gas flow rate were changed. Here, two large magnetic-field coils (greenish-yellow regions) were used, and I_1 (I_2) corresponds to the coil current in the upstream (downstream) side of the device, as shown in Fig. 4. The ratio of I_2/I_1 was fixed as ~0.3 to obtain the magnetic beach condition with a flat magnetic field near the antenna region. Plasma preionization was performed with $f = 12$ MHz and P_{RF} ~40 W (continuous wave) using a full helical antenna (13 cm in axial length). Then, $f = 435$ MHz (also continuous wave), which corresponds to $B = 155$ G for the ECR condition, was applied using a half-helical antenna (3.6 cm in axial length) was applied. Data were obtained without the RF of $f = 12$ MHz, but even though this frequency was applied at the same time with $f = 435$ MHz RF power, n_e was not changed appreciably. According to the dispersion relation [21], the wavelength λ of a wave with $f = 435$ MHz in vacuum is 67 cm, but λ in a plasma deceases as the wave approaches the ECR region from the strong magnetic-field side and/or high n_e. For example, if $B = 200$ G and $n_e = 10^{11}$ cm^{-3}, λ becomes ~6 cm. Therefore, the design of the axial antenna size is important.

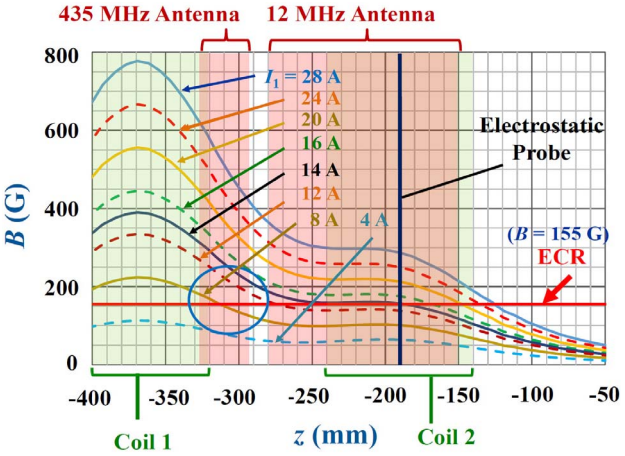

Fig. 4. Axial distributions of the magnetic field, with varying magnetic-field coil currents: from top to bottom, coil 1 current $I_1 = 4$, 8. 12, 14, 16, 20, 24 and 28 A, where I_2 (coil 2 current)/I_1 ~0.3. Here, positions of the magnetic field coils (greenish-yellow regions), two antennas (pink regions), and an electrostatic probe are shown.

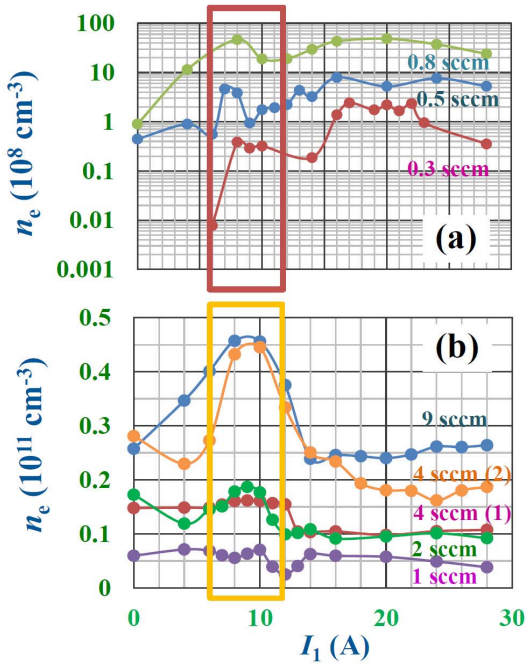

Fig. 5. Electron density n_e as a function of coil 1 current of I_1, changing gas flow rate (a) 0.3, 0.5, and 0.8 sccm. (b) 1, 2, 4, and 9 sccm.

Fig. 5 shows n_e as a function of coil current I_1 (0–28 A), relating to the magnetic-field strength, with the gas flow rate varying from 0.3 to 9 sccm. Below a gas flow rate of 0.3 sccm, plasma could not be produced. Note that n_e data were obtained after stopping the 12-MHz power supply, and typically P_{RF} was ∼110 W with $f = 435$ MHz but was ∼46 W for only one gas flow rate −4 sccm (1)—as shown in Fig. 5. It can be seen from Fig. 5 that near the ECR region, n_e was higher, regardless of gas flow rate (see the circle in Fig. 4 and two boxes in Fig. 5), in most cases. For example, at gas flow rates of 4 and 9 sccm, n_e was increased by a factor of 2.

Although ECR experiments were conducted, absolute value of n_e was lower than those with the nearly same conditions in the case of $f = 50$ and 70 MHz in the mirror (see Fig. 3) and the convergent [9] magnetic field configurations. However, compared to the same $f = 435$ MHz case, n_e was higher with nearly the same gas flow rate (4–5 sccm) due to the hump in the ECR condition [see Figs. 3(b) and 5(b)]. When applying f of 140 MHz instead of 435 MHz, a slight increase of n_e was observed near the ECR region of $B = 50$ G under the divergent field configuration (not shown).

IV. Plasma Characteristics With $D = 0.1$ and 0.3 cm

To produce very small-diameter plasmas, we first installed a quartz tube with an i.d. of 0.3 cm and an axial length of 45.3 cm, as shown in Fig. 6(b). Here, a straight tube with a four-turn antenna having an axial length of 8 cm was connected to an RF power supply with and without a magnetic field (generated using a large magnetic-field coil).

Since the argon pressure in the upstream region (LHS of the quartz tube) is higher than that in the downstream

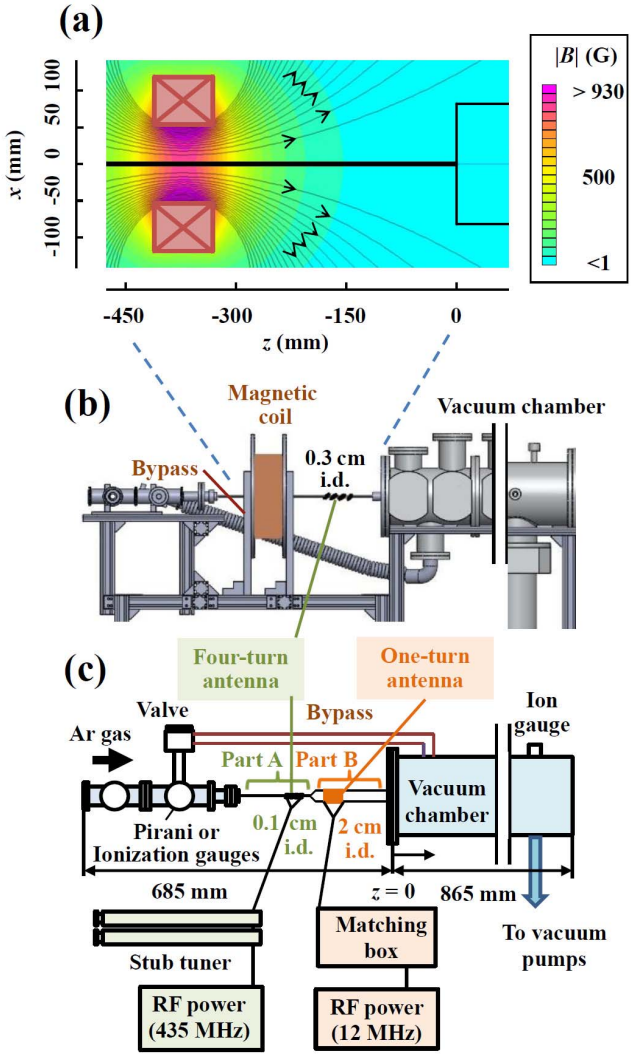

Fig. 6. Experimental setup for very smalldiameter plasma production (a) Magnetic-field profile in the case of $I_c = 30$ A, with i.d. values of (b) 0.3 cm and (c) 0.1 cm.

region [vaccum chamber on right-hand Side (RHS)] owing to the small diameter, yielding a small conductance, a bypass tube (2.65-cm i.d.), as shown in Fig. 6(b) and (c), was installed to lower the pressure in the former, upstream region. Via this bypass method, the pressure in the upstream region was lowered by a factor of ∼200 with the same gas flow rate without the bypass tube for the case of a 0.3-cm i.d. Clearly, it is important to estimate a pressure inside a quartz tube by numerical simulations in future.

Regarding to the magnetic field generated by the electromagnet, in Fig. 6(a), the magnetic-field lines and the field strength are shown in the case of $I_c = 30$ A (use of the larger coil). Although wall effects are important in a small-diameter plasma from the viewpoint of the surface-to-volume ratio, the divergent magnetic field does not play an important role: As shown from Fig. 6(a) (quartz tube has D of 0.3 cm), the radial component of the magnetic field decreases with the decrease of the radius. Thus, an almost straight magnetic configuration is observed in the cases of $D = 0.1$ and 0.3 cm.

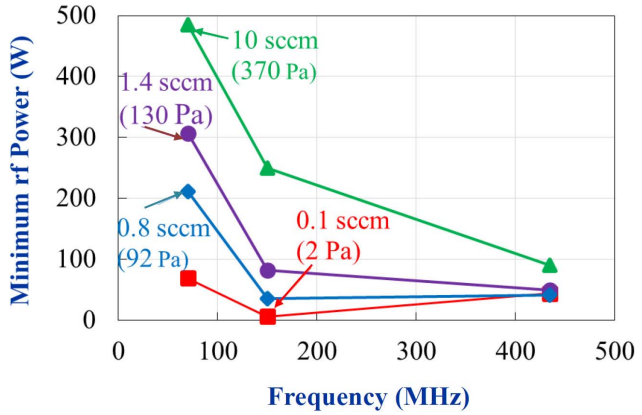

Fig. 7. Minimum RF power for plasma production as a function of the RF frequency, changing gas flow rate (the fill pressure in the upstream region is also shown).

First, operating region of plasma production without a magnetic field was investigated, changing the frequency f and argon pressure P_0 by controlling the gas flow rate, as shown in Fig. 7. In most cases, the minimum P_{RF} for producing the plasma decreased with the increase (decrease) of f (P_0), as shown in Fig. 3.

This advantage of using a higher f can be undertsood partly as follows. If a charged particle oscillates in the RF electric field E_0 in the plasma, the excursion length L in one RF cycle is proportional to E_0/f^2, as can be easily derived from the simple particle equation of motion. For producing a plasma with a small diameter satisfying $L < D$ to prevent wall loss, it is necessary to reduce L, and thus a higher f is necessary. For example, if we use an E_0 of 50 V/m, the L for an electorn is 0.16 (10^{-4}) cm in the case of $f = 12$ (435) MHz. For further discussions, we must consider parameters such as the mean free path, Hall parameter, and an ion Larmor radius. In the case of HP under a magnetic field, according to the dispersion relation of the helicon wave [2], also a higher f is necessary with a smaller diameter if n_e, B and parallel wavenumber are not changed.

Concerning the pressure, it is hard to explain the oberved phenomena quantatively, as the balance between the generation and loss of plasma must be considered numerically. In our case, particle generation (loss) is approximately proportional to the neutral density if the electron-neutral excitation (electron-neutral collision) process is dominant.

Next, n_e as a function of P_{RF} without B was investigated while changing f, as shown in Fig. 8(a), where the tips of Mach probe were located at $z = 2$ cm. The fill pressure P_0 in the upstream region is 3 Pa, and data were obtained from the minimum P_{RF} to produce the plasma. Similar behavior is described in Section III-A for the $D = 2$ cm case; a higher f can produce plasma in the lower P_{RF} region, and n_e in the range of 10^{10} cm^{-3} was obtained with $P_{RF} > 100$ W. The slightly lower n_e compared with Fig. 3 in Section III-A arises from the large distance between the antenna and the probe (24 cm in this case), as well as from the use of the smaller diameter.

Fig. 8(b) shows radial profiles of n_e, changing the axial measuring point, with $f = 12$ MHz and P_{RF} ~1 kW

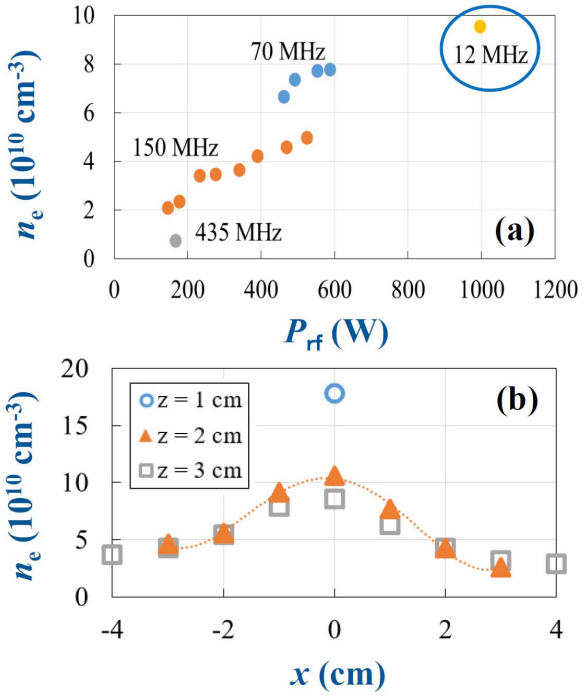

Fig. 8. Electron density n_e as a function of (a) RF power ($P_{Ar} = 3$ Pa), changing RF frequency f, and as a function of (b) radius with $f = 12$ MHz and $P_{RF} \sim 1$ kW [see the blue circle case in Fig 7(a)].

[see the circle in Fig. 8(a)]. It can be seen that $n_e \sim 10^{11}$ cm^{-3} and extends radially with several centimeters in diameter. A sharp (slow) n_e decay from $z = 0$ (1) to 1 (2) cm was observed. If we assume that n_e is inversely proportional to the cross-sectional area and is uniform in the 0.3-cm i.d. tube area (with assumptions of no wall loss and a constant plasma velocity without a source term), the mean n_e in the tube can be as high as $\sim 2 \times 10^{13}$ cm^{-3} according to the data for $z = 2$ and 3 cm with an integration radius ranging from 0 to 3 cm.

In the presence of the magnetic field, n_e increased with a coil current I_c up to 100 A under a pressure of $P_0 = 3$ Pa, where n_e was higher than that without the magnetic field. On the other hand, n_e was almost constant with I_c in the case of $P_0 = 370$ Pa. In this high-pressure range, n_e was also almost constant, regardless of the pressure, i.e., regardless of the gas flow rate. Here, the electron Hall parameter is estimated to be 2.3 (290) for $P_0 = 370$ (3) Pa with $I_c = 30$ A (maximum $B = 860$ G), considering the sum of an electron-neutral collision and a minor contribution of an electron-ion collision. The electron (ion) Larmor radius is estimated to be ~6 × 10^{-3} cm (~0.4 cm) using our typical temperature, which is far smaller (comparable) to the tube diameter. Therefore, the electrons are well-magnetized in the case of $P_0 = 3$ Pa, with I_c significantly exceding 0.1 A, but not magnetized in the high-pressure region.

In the next case, the further smaller diameter discharge was employed, whose experimental setup is shown in Fig. 6(b), without the magnetic field (just recently, we could also produce a plasma with the magnetic field). This 0.1-cm i.d. tube (Part A: 16 cm axial length) was connected to a 2-cm i.d quartz tube (Part B: 15.5-cm axial length). Here, the positions

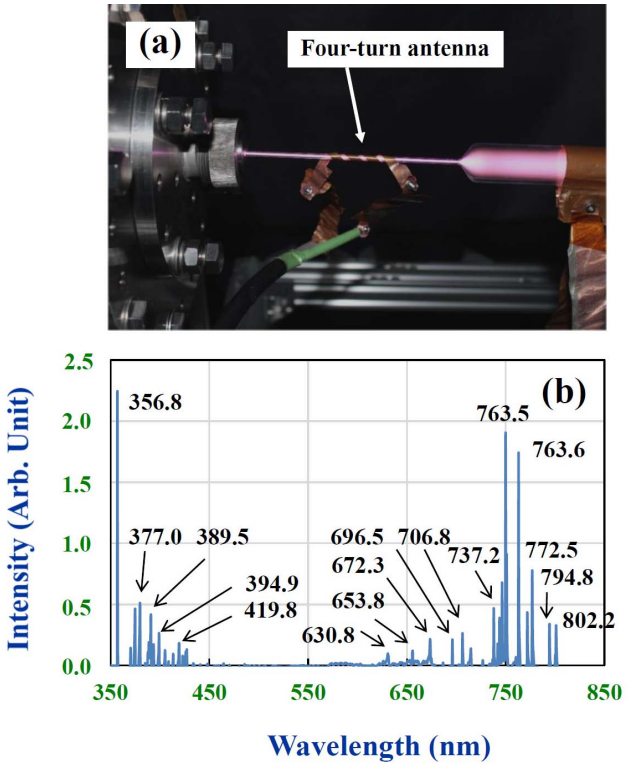

Fig. 9. (a) Photograph in 1mm diameter discharge and (b) Ar spectrum.

of Part A and Part B with antennas, which are described shown below, were exchanged, but no appreciable change in the plasma behaviors was observed between the two cases. In Part A (Part B), a four-turn (one-turn) antenna with an axial length of 4 cm (4 cm) is connected with 435-MHz (12-MHz) power supply for the main plasma production (preionization) with the use of a distributed constant system having two stub tuners (lumped-circuit system having capacitors and inductors). After the plasma ignition with $f = 12$ MHz with a pulsed power of 400 W (duty is 10 %), as previously mentioned, this power was reduced to zero for measuring/estimating n_e: plasma could be still maintained with operation at $f = 435$ MHz and continuous power of 200 W.

Fig. 9(a) shows a photograph of the smallest RF discharge, to our knowledge, under a low-pressure (2.6 Pa in the upstream region) condition. Higher pressure discharges, e.g., 50 and 100 Pa, could also be obtained, by controlling the gas flow rate in the bypass tube. Here, even though there is a large pressure change, gas flow rate was kept constant at 30 sccm, and a constant pressure of ~0.1 Pa was observed near the end of the vacuum chamber, regardless of the flow rate in the bypass tube.

Fig. 9(b) shows the argon spectrum near the antenna region, obtained using the spectrometer. From various Ar I intensities, we derived n_e and T_e using our developed CR model, as mentioned in the introduction. For this pressure case, n_e and T_e are estimated to be high of $\sim 0.5 \times 10^{11}$ cm^{-3} ($\sim 0.8 \times 10^{11}$ cm^{-3}) with ~5 eV (~6 eV) for P_{RF} ($f = 435$ MHz) = 100 W (150 W), respectively, although the accuracy of the CR model under development is unclear. In the higher pressure cases, both $P_0 = 50$ and 100 Pa have shown that n_e and T_e are $\sim 2 \times 10^{11}$ cm^{-3} ($\sim 7 \times 10^{11}$ cm^{-3}) and ~2 eV (~ 2 eV) for P_{RF} = 100 W (150 W) with $f = 435$ MHz, respectively. Accordingly, a pressure higher than 2.6 Pa yielded a higher n_e and lower T_e obtained, as expected.

The contents of the CR model that we developed using rate equations are as follows [27]. The elementary processes include:

1) collisional excitation and its reversal deexcitation due to electron collision;
2) electron collisional ionization;
3) the optical escape factor of the radiative transition, taking into account the optical thickness of the plasma;
4) electron three-body recombinations;
5) radiative and dielectronic recombinatin, in addition to a consideration of two metastable states to describe the diffusion loss and atomic collisional processes.

Here, the number of energy level state p of the Ar I line was taken as 65.

The particle densiy N_p at the state p was derived by inserting n_e, T_e, $P_{0,}$ and neutral temperature T_n (= 300 K). Then, in order to derive the above plasma parameters of n_e and T_e, before hand, we plotted contours of the following ratios in n_e–T_e space, by multiplying A coefficient by N_p: the intensity ratios of I (687.1 nm)/I (763.5 nm), I (603.2 nm)/I (763.5 nm), and I (603.2 nm)/I (687.1 nm). According to the aforementioned results, we could demonstrate the plasma production with a very small dimeter (0.1-cm i.d.) in a wide pressure range (a few Pa to 100 Pa) with n_e of the order of 10^{10}–10^{11} cm^{-3} and T_e ranging from a few to several electronvolts.

Finally, we discuss the particle production efficiency, i.e., the relationship between N_e/P_{RF} and a^2, where N_e is the total number of electrons in the whole plasma region. Good agreement was obtained between the experiments and the theoretical upper limit with an enhancement classical diffusion factor of ~3 [20] (the case where radial diffusion is dominant over axial diffusion) in a very wide range of plasma radius a: 1.25 cm to 38 cm. That is, N_e/P_{RF} was proportional to a^2. If additionally we plot cases with $a = 0.15$–1 cm, for which the scaling still holds well. In addition, even though no magnetic field is applied, $a = 0.05$ cm also obeys this scaling, showing a good particle production efficiency in our experiments.

V. $m = 0$ Half-Cycle Plasma Acceleration

Here, we will describe electrodeless plasma acceleration employing the electromagnetic force. Various schemes proposed have been investigated, and in this paper, $m = 0$ half-cycle acceleration [5] experiment is presented. Fig. 10(a) shows the concept of this scheme (acceleration phase), which employs a low-frequency current I_{ext} applied to the external coil over the first half of a wave period. The basic idea is to induce an azimuthal current j_θ in the presence of a divergent magnetic field to produce the $j_\theta \times B_r$ (radial component of the magnetic field) axial Lorentz force, which is similar to the RMF scheme.

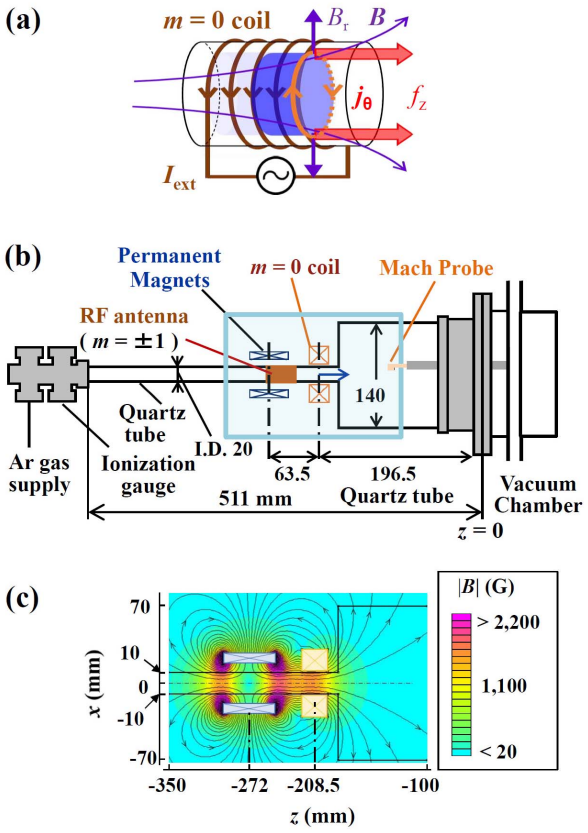

Fig. 10. (a) Concept of the $m = 0$ half-cycle acceleration (acceleration phase), (b) experimental setup for this acceleration scheme, and (c) magnetic field produced by permanent magnets with an $m = 0$ coil current $I_{ext} = 150$ A.

The plasma flow in the negative direction (the latter half of a wave period) does not exert a negative thrust on the spacecraft itself: if the plasma hits the inner wall (total momentum is zero) or the plasma stays in the spacecraft without hitting the wall, it leads to a zero net force in total system eventually. If during the first half-period, the field driven by the antenna is strong enough to push the plasmoid outside of the acceleration region that was localized just under the antenna, a net positive force remains. Here, the necessary experimental conditions for the acceleration were previously discussed in [5].

Figs. 10(b) and (c) show the schematics of the present experimental setup with a high $m = 0$ current ($I_{ext} = 300$ A_{pp}), which is mentioned later, and the strength of the magnetic field with its field lines generated by the permanent magnets and $I_{ext} = 150$ A, respectively, in the case of $D = 2$ cm. In the case of no external $m = 0$ current, the field structures on the RHS can be the same as those on the LHS. The typical axial B_z and radial B_r magnetic fields with $I_{ext} = 0$ near this coil are 200–800 and 20–100 G (at radial position $r \sim 0.5$ cm), respectively, depending on the radial positions. On the other hand, in the phase of positive (negative) antenna current, B_z and B_r increased (decreased) and decreased (increased), respectively, in the LHS axial region of the coil, and both B_z and B_r increased (decreased) in the RHS region.

First, in the case of low coil current I_{ext} of the order of 10 A with $f = 5$ kHz, using an alternating-current power source, experiments were performed according to the configuration of

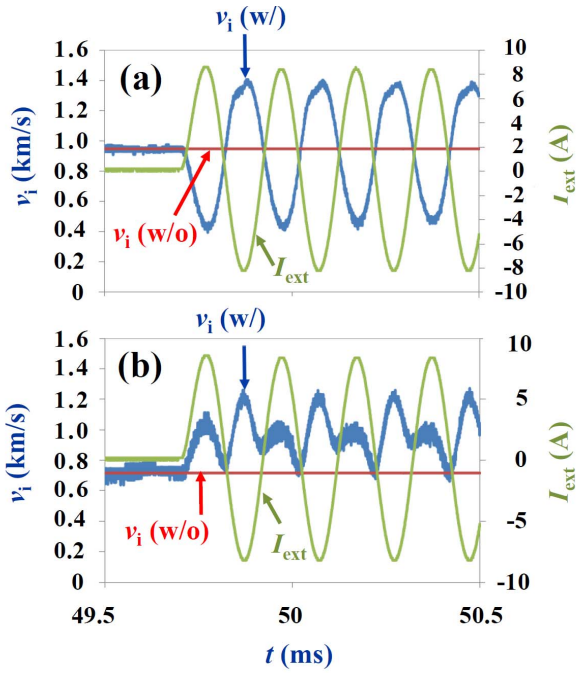

Fig. 11. Time evolutions of the external coil current I_{ext} and ion velocity v_i (with and without I_{ext}). Here, the Mach probe to measure v_i is located at (a) $r = 0$ and (b) 0.6 cm.

Fig. 1 (not Fig. 10 in this experiment). The typical magnetic-field profile is shown in Fig. 6(a) (the lower axial field B is 140 G because $I_c = 5$ A), but the axial position of the magnetic-field coil differs from the present case. The central distance between the large magnetic coil (axial component is $B = 140$ G but radial one is less than a few G depending on the radial position near the $m = 0$ coil) and the $m = 0$ coil (winding of 20 turns) is 7 cm, and a double-loop antenna upstream from the magnetic-field coil, with $f = 12$ MHz and $P_{RF} = 1.5$ kW, was used to produce the plasma.

Fig. 11 shows I_{ext} and v_i [near the $m = 0$ coil region, but at $r = (a)$ 0 and (b) 0.6 cm] with respect to time in an RF discharge with $t = 0$–100 ms ($P \sim 2$ Pa in the head region). In the central radial position [Fig. 11(a)], I_{ext} and v_i are out of phase, as expected from our proposed scheme of the $m = 0$ half-cycle acceleration. Here, I_{ext} and n_e are nearly out of phase, and the relative change of n_e (mean value is $\sim 4 \times 10^{11}$ cm^{-3}) was <40% peak-to-peak. On the other hand, at $r = 0.6$ cm [Fig. 11(b)], v_i was not a sine wave but a full wave (rectifier). This may be related to the ICR combined with the ponderomotive acceleration effect near the plasma surface [28]–[31] or the Faraday accelerator with radio frequency-assisted discharge (FARAD) [32] In the latter case, a very short but large pulsed current is normally utilized for electromagnetic force. Although this is an interesting phenomenon, it needs to be investigated in further detail.

Next, in the case of a high coil current I_{ext} of the order of 100 A with $f \sim 5$ kHz, we fabricated a current driver system, as shown in Fig. 12. There were four modules with insulated gate bipolar transistors (IGBTs), and f was varied by properly choosing the inductors and capacitors in this electric circuit. This power supply was connected to an $m = 0$ coil (30 turns), as shown in Fig. 10(b). There were permanent magnets,

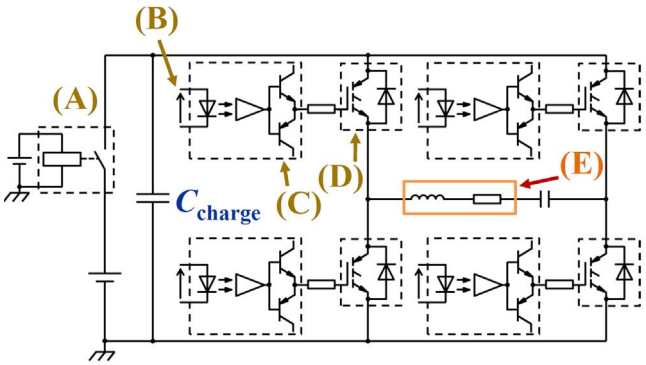

Fig. 12. Driver circuit with four modules for a large current of the $m = 0$ coil (A) relay, (B) external signal, (C) gate driver, (D) IGBT module, and (E) $m = 0$ coil.

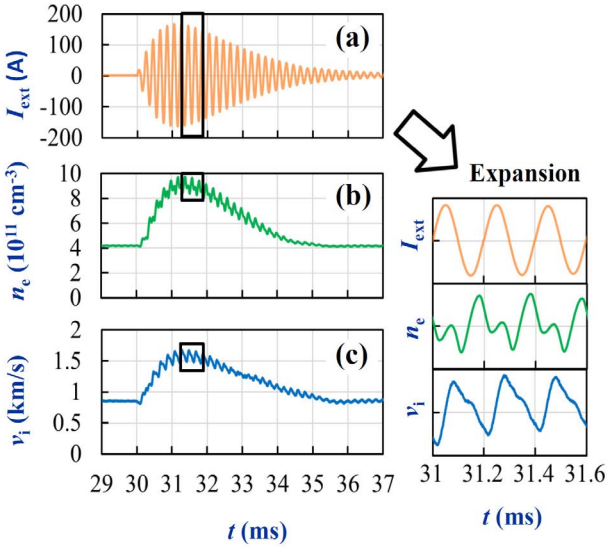

Fig. 13. Time evolutions of (a) external coil current I_{ext}, (b) electron density n_e, and (c) ion velocity v_i. Expanded views of these parameters are shown on the RHS.

whose field was stronger than that of the electromagnets operated in the low-I_{ext} case (these result are shown in Fig. 11). However, the magnitude of the field decreases rapidly as the distance from the permanent magnets increases, compared to the electromagnets.

Fig 13 shows results for the time evolutions of I_{ext}, n_e, and v_i in an RF discharge with $P = 1.1$ Pa in the head region. It can be seen that a mixture of increases of parameters of n_e and v_i with oscillating ones. An increase of n_e (v_i) by a factor of up to 2 (2.3) compared with that without this acceleration phase was observed, along with oscillations. The increase of n_e may arise mainly from the ohmic heating, and encouragingly, the rate of the increase of v_i is higher than that of n_e. We must also note that the mechanism by the FARAD method, as a large coil current is generally necessary. As shown in expanded figures (RHS), the second harmonic was also found. There are some phase shifts between I_{ext}, n_e, and v_i (neither in nor out of phases). These must be investigated together with the measurement of the current j_θ induced in the plasma, in consideration of the power balance.

In the present experiment, the absolute value of v_i was small (here, argon discharge), but it is high in the case of lighter ions such as hydrogen and helium [10]. The axial and radial velocities of v_i obtained using the laser-induced fluorescence method [33], [34] were similar to those in the electrostatic probe data.

VI. Summary

We presented the recent development and characterization of very small-diameter RF plasmas such as HP and MICP, and also presented a trial of $m = 0$ acceleration using small HP source as one of the advanced electromagnetic acceleration methods, considering the future plasma thrusters operating under electrodeless conditions.

Concerning small-diameter RF plasma in a low-pressure condition, we first characterized 2-cm i.d. plasmas under the mirror and divergent magnetic field configurations. In the former case, after a density jump, n_e more than 10^{12} cm^{-3} was obtained, and before the jump, a range of n_e more than 10^{11} cm^{-3} was realized with P_{RF} less than a few 100 W. In this low RF power range, f of 70 or 140 MHz was advantageous from the viewpoint of the particle production efficiency. In the latter case, a higher n_e near the ECR region was indicated over a wide range of the gas flow rate of 0.1–20 sccm, under the conditions of a weaker field and lower frequency—$B = 145$ G and $f = 435$ MHz, respectively—than those generally employed ($B = 875$ G and $f = 2.45$ GHz).

Next, smaller-diameter plasma of 0.3 cm was characterized. Regarding to the minimum RF power for plasma production, a lower gas flow rate and higher f (of the order of 100 MHz), was better. Near the head of the vacuum vessel region (downstream from the production region) connected to the discharge tube, n_e was $\sim 10^{11}$ cm^{-3} with $P_{RF} \sim 1$ kW, which suggests n_e exceeded 10^{13} cm^{-3} in the antenna production region. We succeeded in generating even smaller plasma using under low (2.6 Pa)- and high (50 and 100 Pa)- pressure RF discharges, with the smallest diameter of 0.1 cm. Here, $f = 435$ MHz with $P_{RF} = 100$ and 150 W, and n_e was still high (10^{10}–10^{11} cm^{-3}) according to the calculation based on the CR model. The higher P_0 yielded a higher n_e and lower T_e. Even in the small-diameter case, an excellent particle production efficiency, which obeys the formerly obtained scaling law, was suggested.

Third, $m = 0$ half-cycle electrodeless acceleration with $f \sim 5$ kHz was attempted on the RF (electrodeless) discharged plasma. In the case of a low I_{ext} (10-A range), oscillation of v_i out of phase of I_{ext} was observed, as expected from our proposed scheme, but interesting behavior of a full-wave type was observed near the plasma surface in the radial direction. Further increase of I_{ext} (100-A range) was accompanied by increases of v_i and n_e by factors of $\sim$2.3 and $\sim$2, respectively, with oscillation having second harmonics. These results appear encouraging, although further detailed characterization is necessary, such as the spatio-temporal n_e, v_i, and j_θ induced in the plasma.

Because our results for HP and MICP were obtained using small-diameter plasmas in the initial experiments, they do not represent the future outlook of real prototype thruster with a miniaturized, automated system, especially for the CubeSat type, to support near Earth and deep space missions. However,

we can expect the followings. As mentioned in the introduction, our plasma sources have multiple advantages over the present thrusters, such as its long operation lifetime, high n_e, plasma production down to $D = 0.1$ cm with a low RF power, and flexible external control parameters, e.g., f and B. In the future, concerning RF generator, a lightweight can be achieved using semiconductors, especially based on micro- and nanofabrication. In addition, for easier impedance matching, instead of using variable capacitors C and inductors L, changing f with a fixed C and L may lead to easier operation. Along with the better plasma performance considering many required efficiencies—such as the thrust, thrust/weight to power ratio, specific impulse, and gas utilization—fabrication of prototype thrusters from $3U$ class spacecraft with a good reliability to a smaller size may be expected. Needless to say, the very small HP and MICP sources developed can be applied to a neutralizer to provide enough electron emission current as well as to a combined operation with the present types of thrusters.

To verify and improve these generation and acceleration schemes in electrodeless conditions presented here for application in space, further studies are needed to extend our understanding of the related physical phenomena, leading to a practical prototype thruster. To specify the most appropriate parameter ranges, further flexible and sophisticated measurements are necessary.

ACKNOWLEDGMENT

The authors would like to thank the significant contributions of the late Prof. K. Toki and late Dr. K. P. Shamrai. They would also like to thank E. Tanaka and J. Obunai for conducting the experiments, as well as the HEAT project members for the useful discussions, and Dr. H. Akatsuka for his assistance in developing the CR model.

REFERENCES

[1] R. W. Boswell, "Plasma production using a standing helicon wave," *Phys. Lett. A*, vol. 33, no. 7, pp. 457–458, Dec. 1970.

[2] S. Shinohara, "Propagating wave characteristics for plasma production in plasma processing field," *Jpn. J. Appl. Phys.*, vol. 36, no. 7B, pp. 4695–4703, Jul. 1997.

[3] M. A. Lieberman and A. J. Lichtenberg, *Principles of Plasma Discharges and Materials Processing*. New York, NY, USA: Wiley, 1994.

[4] S. Shinohara *et al.*, "High-density helicon plasma sources: Basics and application to electrodeless electric propulsion," *Trans. Fusion Sci. Technol.*, vol. 63, no. 1T, pp. 164–167, May 2013.

[5] S. Shinohara, H. Nishida, T. Tanikawa, T. Hada, I. Funaki, and K. P. Shamrai, "Development of electrodeless plasma thrusters with high-density helicon plasma sources," *IEEE Trans. Plasma Sci.*, vol. 42, no. 5, pp. 1245–1254, May 2014.

[6] S. Shinohara and T. Tanikawa, "Development of very large helicon plasma source," *Rev. Sci. Instrum.*, vol. 75, no. 6, pp. 1941–1946, Jun. 2004.

[7] S. Shinohara and T. Tanikawa, "Characteristics of a large volume, helicon plasma source," *Phys. Plasmas*, vol. 12, no. 4, pp. 044502-1–044502-4, Apr. 2005.

[8] D. Kuwahara, A. Mishio, T. Nakagawa, and S. Shinohara, "Development of very small-diameter, inductively coupled magnetized plasma device," *Rev. Sci. Instrum.*, vol. 84, no. 10, pp. 103502-1–103502-4, Oct. 2013.

[9] T. Nakagawa, S. Shinohara, D. Kuwahara, A. Mishio, and H. Fujitsuka, "Characteristics of Rf-produced, high-density plasma with very small diameter," in *Proc. JPS Conf.*, vol. 1. 2014, pp. 015022-1–015022-4.

[10] T. Nakagawa, Y. Sato, E. Tanaka, H. Iwaya, D. Kuwahara, and S. Shinohara, "Study on magnetized RF discharge with very small-diameter," *Plasma Fusion Res.*, vol. 10, pp. 3401037-1–3401037-4, May 2015.

[11] K. Toki, S. Shinohara, T. Tanikawa, and K. P. Shamrai, "Small helicon plasma source for electric propulsion," *Thin Solid Films*, vols. 506–507, pp. 597–600, May 2006.

[12] O. V. Batishchev, "Minihelicon plasma thruster," *IEEE Trans. Plasma Sci.*, vol. 37, no. 8, pp. 1563–1571, Aug. 2009.

[13] C. Charles and R. W. Boswell, "Measurement and modelling of a radiofrequency micro-thruster," *Plasma Sour. Sci. Technol.*, vol. 21, no. 2, pp. 022002-1–022002-4, Mar. 2012.

[14] R. G. Jahn, *Physics of Electric Propulsion*. New York, NY, USA: McGraw-Hill, 1968.

[15] V. G. Grigoryan, "Ion sources for space thrusters (invited)," *Rev. Sci. Instrum.*, vol. 67, no. 3, pp. 1126–1131, Mar. 1996.

[16] C. Charles, "Plasmas for spacecraft propulsion," *J. Phys. D, Apply. Phys.*, vol. 42, no. 16, pp. 163001-1–163001-18, Aug. 2009.

[17] E. Ahedo, "Plasmas for space propulsion," *Plasma Phys. Controlled Fusion*, vol. 53, no. 12, pp. 124037-1–124037-18, Dec. 2011.

[18] F. R. C. Díaz, "The VASIMR rocket," *Sci. Amer.*, vol. 283, pp. 90–97, Nov. 2000.

[19] E. A. Bering, III, *et al.*, "Observations of single-pass ion cyclotron heating in a trans-sonic flowing plasma," *Phys. Plasmas*, vol. 17, no. 4, pp. 043509-1–043509-19, Apr. 2010.

[20] S. Shinohara *et al.*, "Development of high-density helicon plasma sources and their applications," *Phys. Plasmas*, vol. 16, no. 5, pp. 057104-1–057104-10, May 2009.

[21] T. H. Stix, *Waves in Plasmas*. New York, NY, USA: AIP, 1992.

[22] Y. Kawai, N. Itagaki, M. Koga, and H. Muta, "Production of low electron temperature ECR plasma," *Surf. Coat. Technol.*, vol. 193, nos. 1–3, pp. 11–16, Apr. 2005.

[23] J. Vlček, "A collisional-radiative model applicable to argon discharges over a wide range of conditions. I. Formulation and basic data," *J. Phys. D, Appl. Phys.*, vol. 22, no. 5, pp. 623–631, May 1989.

[24] S. Waseda, H. Fujitsuka, S. Shinohara, D. Kuwahara, M. Sakata, and H. Akatsuka, "Optical measurements of high-density helicon plasma by using a high-speed camera and monochromators," *Plasma Fusion Res.*, vol. 9, pp. 3406125-1–3406125-4, Jul. 2014.

[25] M. Hudis and L. M. Lidsky, "Directional Langmuir probe," *J. Appl. Phys.*, vol. 41, no. 12, pp. 5011–5016, Nov. 1970.

[26] K.-S. Chung, I. H. Hutchinson, B. Labombard, and R. W. Conn, "Plasma flow measurements along the presheath of a magnetized plasma," *Phys. Fluids B, Plasma Phys.*, vol. B1, no. 11, pp. 2229–2238, Nov. 1989.

[27] J. Mizuochi, T. Sakamoto, H. Matsuura, and H. Akatsuka, "Evaluation of electron energy distribution function in microwave discharge plasmas by spectroscopic diagnostics with collisional radiative model," *Jpn. J. Appl. Phys.*, vol. 49, no. 3, pp. 036001-1–036001-14, Mar. 2010.

[28] I. Y. Dodin, N. J. Fisch, and J. M. Rax, "Ponderomotive barrier as a Maxwell demon," *Phys. Plasmas*, vol. 11, no. 11, pp. 5046–5064, Nov. 2004.

[29] F. Otsuka, T. Hada, S. Shinohara, T. Tanikawa, and T. Matsuoka, "Numerical studies of ponderomotive acceleration and ion cyclotron resonance: Application to next generation electric thrusters," *Plasma Fusion Res.*, vol. 8, pp. 1406012-1–1406012-14, Mar. 2013.

[30] F. Otsuka, T. Hada, S. Shinohara, T. Tanikawa, and T. Matsuoka, "Numerical modeling of electrodeless electric thruster by ion cyclotron resonance/ponderomotive acceleration," *Plasma Fusion Res.*, vol. 8, pp. 2406067-1–2406067-14, Mar. 2013.

[31] F. Otsuka, T. Hada, S. Shinohara, and T. Tanikawa, "Penetration of a radio frequency electromagnetic field into a magnetized plasma: One-dimensional PIC simulation studies," *Earth, Planets Space*, vol. 67, pp. 85-1–85-10, Dec. 2015.

[32] K. A. Polzin, "Comprehensive review of planar pulsed inductive plasma thruster research and technology," *J. Propuls. Power*, vol. 27, no. 3, pp. 513–531, May/Jun. 2011.

[33] R. F. Boivin and E. E. Scime, "Laser induced fluorescence in ar and he plasmas with a tunable diode laser," *Rev. Sci Instrum.*, vol. 74, no. 10, pp. 4352–4360, Oct. 2003.

[34] N. Teshigahara, S. Shinohara, Y. Yamagata, D. Kuwahara, and M. Watanabe, "Development of 2D laser-induced fluorescence (LIF) system in high-density helicon plasma," *Plasma Fusion Res.*, vol. 9, pp. 3406055-1–3406055-4, Jun. 2014.

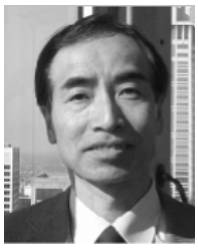

Shunjiro Shinohara received the B.S., M.S., and Ph.D. degrees in physics from the University of Tokyo, Tokyo, Japan, in 1976, 1978, and 1984, respectively.

He has been an Assistant Professor with the Faculty of Science, University of Tokyo since 1980. Then, he became an Associate Professor with the Interdisciplinary Graduate School of Engineering Sciences, Kyushu University, Fukuoka, Japan. He is currently a Distinguished Professor with the Division of Advanced Mechanical Systems Engineering, the Institute of Engineering, Tokyo University of Agriculture and Technology, Tokyo. His current research interests include extensive plasma science including RF discharges (such as helicon discharge), plasma propulsion, nonlinear physiscs such as bifurcation, self-organization, and turbulent studies, and also the beavior of Mangetohydrodynamic in high-temperature plasma/nuclear fusion fields.

Prof. Shinohara received the Commendation for Science and Technology by the Minister of Education, Culture, Sports, Science and Technology, Japan, in 2010, and the Notable Contribution to Technology by the Japan Society of Plasma Science and Nuclear Fusion Research in 2016.

Daisuke Kuwahara was born in Shizuoka, Japan, in 1984. He received the B.E. degree from the Department of Electrical and Electronic Engineering, Undergraduate School of Engineering Science, Toyohashi University of Technology, Aichi, Japan, in 2007, and the M.E. and Ph.D. degrees in engineering from the Department of Energy Science, Interdisciplinary Graduate School of Science and Engineering, Tokyo Institute of Technology, Tokyo, Japan, in 2009 and 2012, respectively.

He has been an Assistant Professor with the Division of Advanced Mechanical Systems Engineering, the Institute of Engineering, Tokyo University of Agriculture and Technology, Tokyo, since 2012. His current research interests include development of a helicon plasma thruster.

Takamichi Ishii was born in Nagano, Japan, in 1990. He received the B.E. degree from the Department of Mechanical Systems Engineering, Faculty of Engineering, and the M.E. degree from the Department of Mechanical Systems Engineering, Graduate School of Engineering, Tokyo University of Agriculture and Engineering, Tokyo, Japan, in 2012 and 2014, respectively.

His current research interests include acceleration of very small RF plasma sources.

Hiraku Iwaya was born in Chiba, Japan, in 1992. He received the B.E. degree from the Department of Mechanical Systems Engineering, Faculty of Engineering, and the M.E. degree from the Department of Management of Technology, Graduate School of Engineering, Tokyo University of Agriculture and Engineering, Tokyo, Japan, in 2015 and 2017, respectively.

His current research interests include small RF plasma sources under a low gas pressure with a wide excitation frequency range, as well as the electron cyclotron resonance plasma production with the low magnetic field.

Shuichi Nishimura was born in Fukuoka, Japan in 1993. He received the B.E. degree from the Department of Mechanical Systems Engineering, Faculty of Engineering, Tokyo University of Agriculture and Technology, Tokyo, Japan, in 2016, where he is currently pursuing the M.E. degree with the Department of Mechanical Systems Engineering, Graduate School of Engineering, Tokyo University of Agriculture and Technology.

His current research interests include acceleration of a developed small RF plasma source.

Tomoya Yamase was born in Kochi, Japan, in 1993. He received the B.E. degree from the Department of Mechanical Systems Engineering, Faculty of Engineering, Tokyo University of Agriculture and Technology, Tokyo, Japan, in 2016, where he is currently pursuing the M.E. degree with the Department of Mechanical Systems Engineering, Graduate School of Engineering, Tokyo University of Agriculture and Technology.

His current research interests include development of very small RF plasma sources.

Daisuke Arai was born in Kagawa, Japan, in 1995. He received the B.E. degree from the Department of Mechanical Systems Engineering, Faculty of Engineering, Tokyo University of Agriculture and Technology, Tokyo, Japan, in 2017, where he is currently pursuing the M.E. degree with the Department of Mechanical Systems Engineering, Graduate School of Engineering, Tokyo University of Agriculture and Technology.

His current research interests include development of small RF plasma thruster.

Hirotaka Horita was born in Chiba, Japan, in 1994. He received the B.E. degree from the Department of Mechanical Systems Engineering, Faculty of Engineering, Tokyo University of Agriculture and Technology, Tokyo, Japan, in 2017, where he is currently pursuing the MOT degree with the Department of Industrial Technology and Innovation, Graduate School of Engineering, Tokyo University of Agriculture and Technology.

His current research interests include the development of plasma spectral measurement.